

LASER TRANSFERRED HYDROUS RUTHENIUM OXIDE ELECTRODES FOR MICRO-ULTRACAPACITORS

Craig B. Arnold, Karen E. Swider-Lyons and Alberto Piqué
Naval Research Laboratory
Washington, DC 20375, USA

Abstract

Hydrous ruthenium oxide ($\text{RuO}_2 \cdot 0.5 \text{H}_2\text{O}$) electrodes have been deposited under ambient conditions using a laser transfer process. The transferred material exhibits a porous, high surface area morphology that is ideally suited for micro-ultracapacitor electrodes. Electrochemical evaluation of single electrodes via cyclic voltammetry (CV) reveals that the laser transfer process does not adversely affect the electrochemical properties of the $\text{RuO}_2 \cdot 0.5 \text{H}_2\text{O}$. The CV curves exhibit constant current behavior with high specific capacitance. As the scan rate is increased, there is a slight decrease in the specific capacitance that is comparable to previously reported data. The specific capacitance decreases only 23 % between $5 \text{ mV} \cdot \text{s}^{-1}$ and $100 \text{ mV} \cdot \text{s}^{-1}$. In situ laser micromachining is used to shape the deposited electrode material into planar micro-ultracapacitor cells that show excellent charge storage as well as high discharge current capabilities.

INTRODUCTION

Electrical energy storage is required for many applications ranging from consumer products and telecommunication devices to electric/hybrid vehicles and stand-by power systems. For applications in which significant power is needed in long pulses, neither batteries nor traditional capacitors are capable of delivering the required peak powers (1, 2, 3). The use of high capacitance electrochemical capacitors (ultracapacitors or supercapacitors) offers a viable alternative for such applications because their ability to deliver high power for extended durations. The need for pulsed power is also critical for the operation of autonomous microelectronic systems such as microsensors and transmitters or micro-electromechanical systems (MEMS) (4). The size constraints of such microdevices require power sources with high energy and power per unit mass and/or volume in a package of commensurate size. These requirements are unable to be met by the current generation of microbatteries or micro-fuel cells alone (4, 5).

Amorphous hydrous ruthenium oxide ($\text{RuO}_2 \cdot x \text{H}_2\text{O}$) is an ideal electrode material for a micro-ultracapacitor as it is one of the highest specific capacitance materials available (720 F/g for $x=0.5$) (6). The rapid and double insertion and release of protons and electrons in the RuO_2 leads to a large pseudocapacitance effect, which, in combination with a high specific surface area, leads to the high amounts of charge storage by the material (6, 7, 8). This pseudocapacitance effect is enhanced by the presence of structural water in the lattice which provides nanostructured percolation pathways for proton conduction into the bulk of

the material (9). The capacitance of the $\text{RuO}_2 \cdot x \text{H}_2\text{O}$ sensitively depends on the processing temperature through the loss of structural water, and it is maximized when the hydrous material is heated to $\sim 150\text{-}170^\circ\text{C}$ with a chemical formula of $\text{RuO}_2 \cdot 0.5 \text{H}_2\text{O}$ (6, 9, 10).

Hydrous ruthenium oxide electrodes are typically produced by rolling or pressing sol-gel derived powders combined with approximately 5 wt.% binder such as teflon (6, 11). In other work, composite powders of ruthenium oxide and carbon have been produced through electroless deposition (12), colloidal processes (13), or sol-gel techniques (14) and then used to form electrodes. Although rolling and pressing electrodes is acceptable for producing large-scale, monolithic ultracapacitors or even thin film ultracapacitors, these techniques are not suitable for integrated devices or on-chip manufacturing. Other approaches have been developed recently to directly deposit hydrous ruthenium oxide electrode material on to substrates, including electrostatic spray deposition (15) as well as sol-gel techniques (16).

In recent work, we have demonstrated the ability to deposit high capacity $\text{RuO}_2 \cdot 0.5 \text{H}_2\text{O}$ micro-ultracapacitor electrodes using a laser forward transfer process (17, 18). Laser forward transfer is considered a direct-write technique in that material is deposited only where desired. One of the main advantages of the laser technique is that we are able to immediately process the deposited electrode through laser micromachining into compositionally symmetric planar micro-ultracapacitor cells using the same apparatus. There is no need for any ex-situ patterning to be done. In contrast to other film deposition techniques, our technique incorporates electrolyte directly into the electrode during deposition without the need to remove reacted species from the deposited film. Specific power greater than 1000 mW/g and energies $> 10 \text{ mWhr/g}$ were obtained in cells weighing less than 100 μg with volumes as small as $3 \times 10^{-5} \text{ mL}$.

In this paper, we examine the details of the hydrous ruthenium oxide electrode material deposited by laser transfer (LT) and compare them to electrodes prepared by other techniques such as conventional pressing and rolling, and stenciling. The laser transfer process preserves the morphology of the initial hydrous material and we find the electrochemical properties of LT $\text{RuO}_2 \cdot 0.5 \text{H}_2\text{O}$ to be comparable to those of conventional methods with better specific capacitance at high voltage scan rates.

EXPERIMENTAL SETUP

Hydrous ruthenium oxide is deposited using a patented laser direct-write technique developed at the Naval Research Laboratory (19, 20, 21). Commercially available hydrous ruthenium oxide powder (Alfa-Aesar, $\text{RuO}_2 \cdot 2.5 \text{H}_2\text{O}$) is oven heated to 150°C for 18 hours to yield a material with the desired water content of 0.5 mol H_2O per mol RuO_2 for optimal charge storage (6). The dry powder is combined with 5 M sulfuric acid to form a suspension or ink, which is spread using a wire-coater (# 6 Garner) on a borosilicate plate forming an approximately 5 μm thick coating. The $\text{RuO}_2 \cdot 0.5 \text{H}_2\text{O} + \text{H}_2\text{SO}_4$ ink is irradiated through the back of the borosilicate plate using a frequency-tripled Nd:YAG laser ($\lambda=355 \text{ nm}$) to induce the forward transfer of material to a substrate $\sim 100 \mu\text{m}$ below

the ribbon. An accurate measurement of the mass of the transferred material is made using a microbalance (Sartorius M2P) with μg resolution.

For half-cell measurements of single electrodes, graphite foil (Alfa-Aesar) is cut into thin strips (5 mm x 20 mm x 0.25 mm) to be used as a substrate material for the transferred hydrous ruthenium oxide. We deposit single electrodes nominally of $\text{RuO}_2 \cdot 0.5 \text{H}_2\text{O} + \text{H}_2\text{SO}_4$ (2.25 mm x 2.25 mm x 15 μm) on each graphite substrate, and subsequently drop cast a 5% Nafion[®] ionomer solution (Ion Power, Liquion 1100) over the electrode. The solution is allowed to dry at room temperature, resulting in a continuous Nafion film that prevents electrode delamination during testing. As a control experiment, we prepare similar sized electrodes on graphite foil by stenciling the $\text{RuO}_2 \cdot 0.5 \text{H}_2\text{O}$ ink through a laser machined polyimide mask.

Planar micro-ultracapacitor cells are constructed on 1 cm x 1 cm gold-coated quartz wafers, on which we electrically isolate four current collector pads by UV laser micromachining 20 μm grooves in the surface. Hydrous ruthenium oxide films, approximately 1 mm x 2 mm x 15- μm thick, are then deposited across the machined groove in the gold. An infrared laser ($\lambda = 1064 \text{ nm}$) is used to locally dry the deposited material and a 20 μm wide line is UV laser machined across the $\text{RuO}_2 \cdot 0.5 \text{H}_2\text{O}$ film to establish a symmetric planar ultracapacitor with two identical 0.5 mm x 2 mm x 15 μm electrodes. Nafion film is drop cast on to the micro-ultracapacitor cell and allowed to air dry to prevent electrode delamination.

We electrochemically evaluate the hydrous ruthenium oxide through cyclic voltammetry (CV) and chronopotentiometry (CP) carried out using an EG&G PAR potentiostat (Model 263). For cyclic voltammetry, the single electrode on graphite foil is submerged in a solution of 0.5 M H_2SO_4 in a standard three electrode configuration using platinum mesh as a counter electrode and a Pd/H reference electrode. The reference electrode is prepared by cleaning a Pd wire in concentrated nitric acid before charging it with hydrogen through electrolysis of water in an acidic solution for 5 minutes. Various scan rates are examined over the potential range of 0 to 1000 mV vs normal hydrogen electrode (NHE). For chronopotentiometry on the full micro-ultracapacitor cells, a droplet of 0.5 M H_2SO_4 is placed on top of the Nafion coated micro-ultracapacitor cell and the cell is connected to the potentiostat through a probe station. Data is acquired at specified currents for potentials between 0 and 1 V in this two-electrode configuration.

RESULTS AND DISCUSSION

LT hydrous ruthenium oxide electrodes maintain their morphological and electrochemical properties in comparison to electrodes formed by stenciling. Figure 1 shows scanning electron microscopy (SEM) images of the initial $\text{RuO}_2 \cdot 0.5 \text{H}_2\text{O}$ powder, stenciled $\text{RuO}_2 \cdot 0.5 \text{H}_2\text{O}$ and LT $\text{RuO}_2 \cdot 0.5 \text{H}_2\text{O}$. The stenciled and LT samples are heated on a hot plate to 150 $^\circ\text{C}$ and cooled prior to microscopy to evaporate the excess water from the material. The powder and stenciled material exhibit a high surface area with porous microstructure, as expected for the high capacity $\text{RuO}_2 \cdot 0.5 \text{H}_2\text{O}$ system. Under these high

magnification images, it is apparent that the laser transfer technique does not harm the desirable morphological properties as there are no indications of melted or fractured material on these length scales.

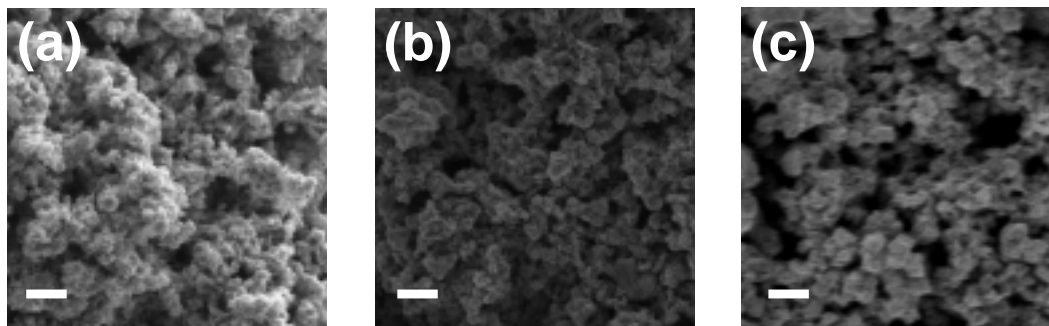


Figure 1. High magnification SEM images of (a) $\text{RuO}_2 \cdot 0.5 \text{H}_2\text{O}$ powder, (b) stenciled material (c) laser transferred material. Scale is the same in all images with scale bar representing 300 nm.

Figure 2(a) and (b) show CV curves from a LT electrode scanned at $5 \text{ mV}\cdot\text{s}^{-1}$ and $50 \text{ mV}\cdot\text{s}^{-1}$, respectively, over the potential window of 0-1000 mV in 0.5 M H_2SO_4 . Open circuit potentials for these samples typically ranged between 800-900 mV. The geometric area of this electrodes is measured in an optical microscope to be 5 mm^2 . At lower scan rates, voltammetry curves show nearly constant current behavior over the potential window, indicative of the ideal capacitive behavior of the $\text{RuO}_2 \cdot 0.5 \text{H}_2\text{O}$ system as previously reported (6, 15). The CV for LT electrodes is in qualitative agreement with that from a stenciled sample as shown in figure 2(c) and (d). Since the stenciled material has not been laser irradiated, this agreement suggests that the laser interaction with the $\text{RuO}_2 \cdot 0.5 \text{H}_2\text{O}$ ink does not adversely affect electrochemical properties of the deposited electrode.

The reason our laser transfer process does not damage the morphological or electrochemical properties of the $\text{RuO}_2 \cdot 0.5 \text{H}_2\text{O}$ is that the majority of the transferred material does not interact with the laser. The laser interacts with and is absorbed by a relatively small layer of material at the interface between the borosilicate glass plate and the ruthenium oxide ink. Energy absorption occurs on nanometer length scale in comparison to the micron scale thickness of the ink layer. This small volume of material is rapidly heated and vaporized creating a pressure front that pushes the material out of the ink layer and to the substrate below (22). The energetics of the laser interaction process in addition to the rheological properties of the ink affect the momentum as well as the spatial distribution of transferred material.

In contrast to earlier work on hydrous ruthenium oxide electrodes (23), there is little difference in the voltammetric features of the LT $\text{RuO}_2 \cdot 0.5 \text{H}_2\text{O}$ electrodes when scanned at $50 \text{ mV}\cdot\text{s}^{-1}$ vs. $5 \text{ mV}\cdot\text{s}^{-1}$ (figure 2(a) and (b)). There exists a single broad peak on both the anodic and cathodic sweeps of the CV for LT and stenciled electrodes. The evolution of the CV curve as a function of scan rate is more easily observed in the capacitance behavior. Capacitance of the electrode material is derived by normalizing the current, I , by the voltage scan rate, s , $C = \frac{I}{s}$. The capacitance for different scan rates is shown in figure 3.

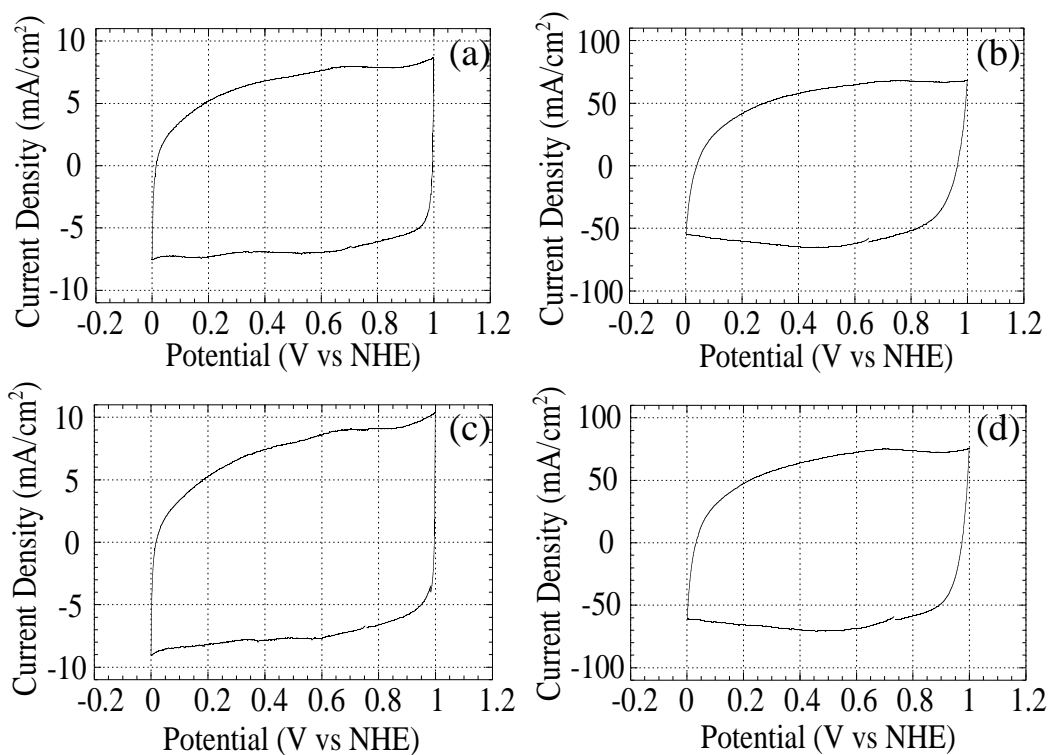


Figure 2. Cyclic Voltammetry for laser transferred and stenciled $\text{RuO}_2 \cdot 0.5 \text{H}_2\text{O}$ electrode material in 0.5 M H_2SO_4 at ambient temperature. (a) $5 \text{ mV}\cdot\text{s}^{-1}$ laser transferred, (b) $50 \text{ mV}\cdot\text{s}^{-1}$ laser transferred, (c) $5 \text{ mV}\cdot\text{s}^{-1}$ stenciled and (d) $50 \text{ mV}\cdot\text{s}^{-1}$ stenciled. The area of the laser transferred electrode is 5 mm^2 and that of the stenciled sample is 3 mm^2 , while the mass of $\text{RuO}_2 \cdot 0.5 \text{H}_2\text{O}$ is $85 \mu\text{g}$ and $50 \mu\text{g}$, respectively.

At lower scan rates the current rapidly changes from oxidizing to reducing (and vice versa) at the vertices indicating sufficient mobility of protons in the electrode in these regimes. However, at scan rates higher than $10 \text{ mV}\cdot\text{s}^{-1}$, the proton mobility becomes a limiting mechanism, leading to a more gradual current change at the vertices and subsequent lower average capacitances (23).

Figure 4 shows the specific capacitance (capacitance normalized by mass) as a function of scan rate for hydrous ruthenium oxide electrodes. We calculate the specific capacitance by averaging the capacitance of the oxidation portion of the CV curve over the entire potential window of 1000 mV and dividing by the mass of $\text{RuO}_2 \cdot 0.5 \text{H}_2\text{O}$ in the electrode. It should be noted that there is a large degree of uncertainty in calculating the mass of $\text{RuO}_2 \cdot 0.5 \text{H}_2\text{O}$ in the LT electrodes. Although the mass of the deposited material is measured, the composition of this material is not necessarily the same as the initial ruthenium oxide / sulfuric acid mixture since relative amounts of these components are affected by laser vaporization and evaporation during the laser transfer process. Based on mass calibrations of transferred material, we find approximately 20 % of the material is volatilized during transfer. Assuming none of the volatilized material is $\text{RuO}_2 \cdot 0.5 \text{H}_2\text{O}$, we obtain a mass of $87 \mu\text{g}$ for the sample in figure 4.

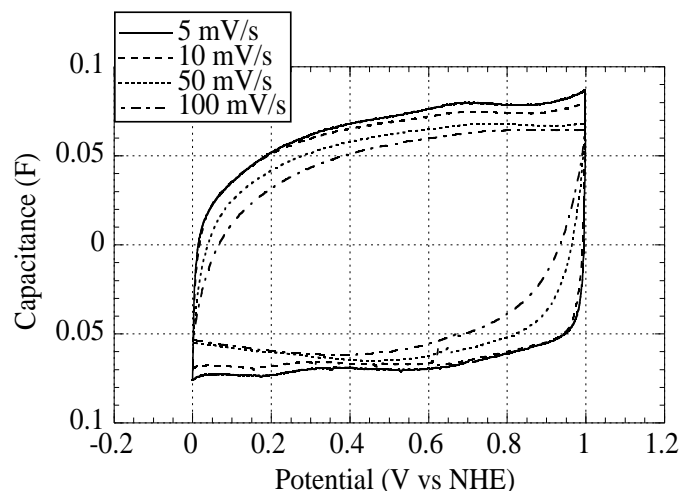


Figure 3. Capacitance versus potential for scan rates of 5, 10, 50 and 100 $\text{mV}\cdot\text{s}^{-1}$ on an LT $\text{RuO}_2 \cdot 0.5 \text{H}_2\text{O}$ electrode. Electrode area is 5 mm^2 and mass of $\text{RuO}_2 \cdot 0.5 \text{H}_2\text{O}$ is $87 \mu\text{g}$.

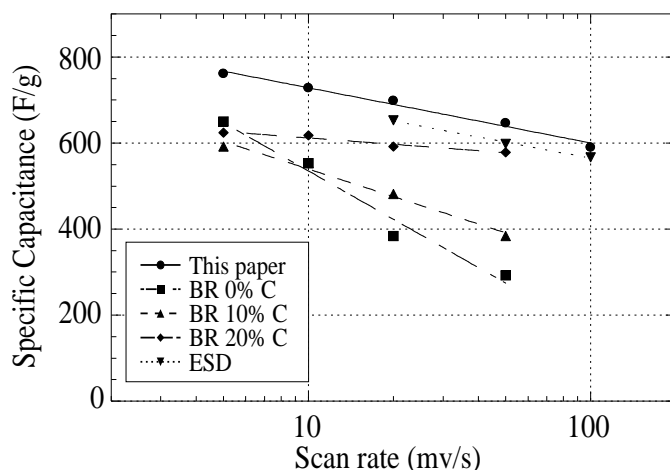


Figure 4. Specific capacitance as a function of scan rate for our experiment in comparison to results from the literature. The circles represent the data from the present work, BR: rolled electrodes with teflon binder and 0, 10, and 20 % C (from reference (23)), ESD: Electrostatic spray discharge (from reference (15)).

The specific capacitance of the LT electrode slowly decays as a function of scan rate. At scan rates as high as $100 \text{ mV}\cdot\text{s}^{-1}$, the LT electrodes maintain over 77 % of the capacity measured at $5 \text{ mV}\cdot\text{s}^{-1}$. This high rate capacity is comparable to previously reported results for $\text{RuO}_2 \cdot 0.5 \text{H}_2\text{O}$. Figure 4 gives specific capacitance data from the literature for other methods of electrode production, including binder addition and rolling (BR) electrodes loaded with activated carbon (23) and electrostatic spray deposition (ESD) electrodes (15). Results for the LT electrodes are most similar in slope to the ESD electrodes and the BR electrodes with 10% carbon.

The main cause of decreased capacitance with scan rate in the hydrous ruthenium

oxide system is the depletion and oversaturation of protons from the electrolyte within the electrode material during rapid reduction and oxidation respectively (23). However, for the highly porous microstructure shown in figure 1(c), there are ample pathways for electrolyte diffusion and penetration in the electrode. Furthermore, initially mixing the sulfuric acid with the $\text{RuO}_2 \cdot 0.5 \text{H}_2\text{O}$ results in the even distribution of the electrolyte throughout the bulk of the electrode and eliminates a source for impurities from reacted species, further enhancing the ability for the electrolyte to deliver protons to the interior of the electrode. It has been shown that directly mixing sulfuric acid with electrode materials increases the charge storage capabilities for LT $\text{RuO}_2 \cdot 0.5 \text{H}_2\text{O}$ (17).

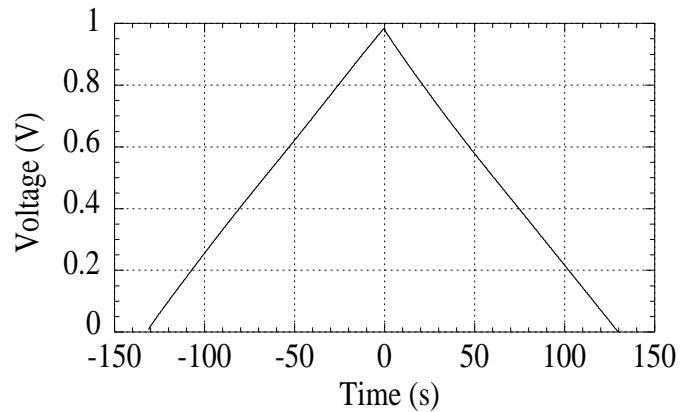


Figure 5. Chronopotentiometry for micro-ultracapacitor cell charged and discharged at $50 \mu\text{A}$ ($0.16 \text{ A}\cdot\text{cm}^{-2}$). The mass of the cell is $80 \mu\text{g}$ with a footprint of 2 mm^2 and thickness of $15 \mu\text{m}$.

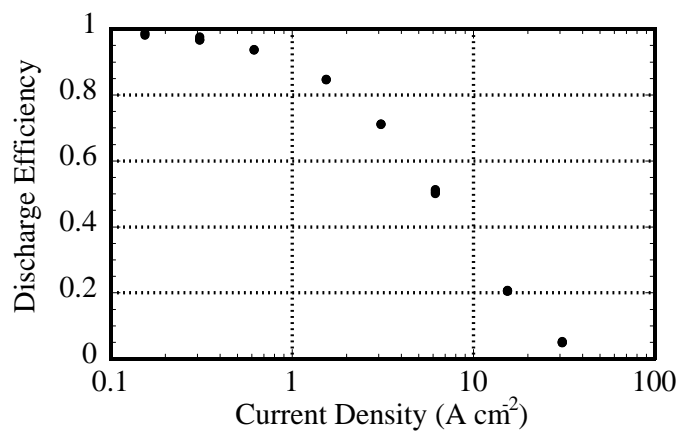


Figure 6. Ratio of extracted charge to stored charge as a function of discharge current density for micro-ultracapacitor cell charged at $50 \mu\text{A}$.

Figure 5 shows chronopotentiometry for a micro-ultracapacitor cell that has been charged and discharged at $50 \mu\text{A}$. The data exhibits linear behavior as expected for an ideal capacitor. As the discharge current is increased for a fixed charging current, the amount of extracted charge decreases. Figure 6 shows the discharge efficiency, defined as

the ratio of the total charge extracted from the cell during discharge to the charge stored during charging at a fixed current. At discharge current densities of $1.5 \text{ A}\cdot\text{cm}^{-2}$, the cells maintain 85 % of their capacity at current densities of $0.15 \text{ A}\cdot\text{cm}^{-2}$. In these measurements for current density, we have normalized the discharge current by the area of the interface between the two electrodes in our planar configuration. The interface area of the cell is $3.1 \times 10^{-4} \text{ cm}^2$, where we have neglected any contributions of porosity to the area. Our results are in agreement with those reported by Zheng for an ultracapacitor made from pressed composite electrodes (23).

SUMMARY

Hydrous ruthenium oxide micro-ultracapacitor electrodes have been produced using a laser transfer process. The transfer process preserves the morphological and electrochemical properties of the initial material, resulting in high surface area, porous electrodes with high specific capacitance. The behavior of these electrodes in half cell measurements is consistent with previously reported results for the hydrous ruthenium oxide system. At scan rates greater than $10 \text{ mV}\cdot\text{s}^{-1}$, the CV data shows a decrease in capacitance, however, it is a smaller effect than that observed for conventionally rolled electrodes. The specific capacitance shows a small scan rate dependence with over 77 % efficiency at $100 \text{ mV}\cdot\text{s}^{-1}$. Planar micro-ultracapacitors are produced by laser micromachining the transferred hydrous material into the two symmetric electrodes. The charging and discharging behavior of these cells show ideal capacitor behavior demonstrating the viability of our laser technique. The discharge efficiency for the micro-ultracapacitor cell demonstrates the ability to attain high discharge current densities while maintaining good energy storage properties in a micro-ultracapacitor.

ACKNOWLEDGEMENTS

This research was supported in part by the Office of Naval Research. CBA acknowledges the support of the National Research Council Postdoctoral Associate Program.

REFERENCES

1. B. E. Conway, *Electrochemical Supercapacitors, Scientific Fundamentals and Technological Applications*, Kluwer Academic, New York, (1999).
2. A. Burke, *J. Power Sources*, **91**, 37 (2000).
3. R. Kotz and M. Carlen, *Electrochimica Acta*, **45**, 2483 (2000).
4. J. N. Harb, R. M. LaFollette, R. H. Selfridge, and L. L. Howell, *J. Power Sources*, **104**, 46 (2002).
5. J. B. Bates, N. J. Dudney, B. Neudecker, A. Ueda, and C. D. Evans, *Solid State Ionics*, **135**, 33 (2000).
6. J. P. Zheng, P. J. Cygan, and T. R. Jow, *J. Electrochem. Soc.*, **142**, 2699 (1995).

7. S. Sarangapani, B. Tilak, and C. Chen, *J. Electrochem. Soc.*, **143**, 3791 (1996).
8. S. Trasatti and P. Kurzweil, *Plat. Met. Rev.*, **38**, 46 (1994).
9. W. Dmowski, T. Egami, K. E. Swider-Lyons, C. T. Love, and D. R. Rolison, *J. Phys. Chem. B*, **106**, 12677 (2002).
10. D. A. McKeown, P. L. Hagans, L. P. L. Carette, A. E. Russell, K. E. Swider, and D. R. Rolison, *J. Phys. Chem. B*, **103**, 4825 (1999).
11. D. A. Evans, J. P. Zheng, and S. L. Roberson, In *Proceedings of the 9th International Seminar on Double Layer Capacitors and Similar Energy Storage Devices*, Deerfield Beach, FL (1999).
12. M. Ramani, B. S. Haran, R. E. White, and B. N. Popov, *J. Electrochem. Soc.*, **148**, A374 (2001).
13. H. Kim and B. N. Popov, *J. Power Sources*, **104**, 52 (2002).
14. Y. Sato, K. Yomogida, T. Nanaumi, K. Kobayakawa, Y. Ohsawa, and M. Kawai, *Electrochem. Solid-State Lett.*, **3**, 113 (2000).
15. I. H. Kim and K. B. Kim, *Electrochem. Solid-State Lett.*, **5**, A62 (2001).
16. Q. L. Fang, D. A. Evans, S. L. Roberson, and J. P. Zheng, *J. Electrochem. Soc.*, **148**, A833 (2001).
17. C. B. Arnold, R. C. Wartena, B. Pratap, K. E. Swider-Lyons, and A. Piqué, In *Electroactive Polymers and Rapid Prototyping*, D. B. Chrisey and S. C. Danforth, Editors, PV 689, p. 275, Materials Research Society, Pittsburgh, PA (2002).
18. C. B. Arnold, R. C. Wartena, K. E. Swider-Lyons, and A. Piqué, *J. Electrochem. Soc.* (*in press*).
19. D. B. Chrisey, R. A. McGill, and A. Piqué, *U.S. Patent No. 6,177,151* (1999).
20. A. Piqué, D. B. Chrisey, J. M. Fitz-Gerald, R. A. McGill, R. C. Y. Auyeung, H. D. Wu, S. Lakeou, V. Nguyen, R. Chung, and M. Duignan, *J. Mater. Res.*, **15**, 1872 (2000).
21. D. B. Chrisey, A. Piqué, J. Fitz-Gerald, R. C. Y. Auyeung, R. A. McGill, H. D. Wu, and M. Duignan, *Appl. Surf. Sci.*, **154-155**, 593 (2000).
22. D. Young, R. C. Y. Auyeung, A. Piqué, D. B. Chrisey, and D. D. Dlott, *Appl. Phys. Lett.*, **78**, 3169 (2001).
23. J. P. Zheng, *Electrochem. Solid-State Lett.*, **2**, 359 (1999).